Asociación Argentina
de Mecánica Computacional

Mecánica Computacional Vol XXXIX, págs. 429-441 (artículo completo)
F.E. Dotti, M. Febbo, S.P. Machado, M. Saravia, M.A. Storti (Eds.)
Bahía Blanca, 1-4 Noviembre 2022

# STUDY OF THE SUPER-LATE STAGE OF THE TEMPORAL TRANSITION IN A PLANE CHANNEL FLOW

**William I. Machaca Abregu**[a, b], **Enzo A. Dari**[a, b, c] **and Federico E. Teruel**[a, b, c]

[a]*Departamento de Mecánica Computacional, Centro Atómico Bariloche, CNEA, Bariloche, Argentina, william.machaca@ib.edu.ar, http://mecom.cnea.gov.ar/*

[b]*Instituto Balseiro, Centro Atómico Bariloche, CNEA-UNCUYO, Bariloche, Argentina*

[c]*CONICET, Centro Atómico Bariloche, CNEA, Bariloche, Argentina*

**Keywords:** Temporal transition, super-late stage, friction coefficient, plane channel flow, DNS, Xcompact3d.

**Abstract.** In this work a temporal laminar-turbulent K-type transition at a subcritical Reynolds number ($Re$ = 5000) is simulated employing Direct Numerical Simulation (DNS). The configuration is a temporal developing channel flow driven by a constant flow rate. The study focuses in the description of flow features before and after the time that corresponds to the peak in the evolution of the friction coefficient during the transition. Specifically, the evolution of the friction coefficient is described employing the FIK identity, vortex structures, and the turbulent kinetic energy budget. Results show that during the peak zone the intensity of the Reynolds shear stress term of the FIK identity is greater than that computed in the fully developed turbulent regime. Also, a peak is found in the temporal evolution of the magnitude of the turbulent dissipation in this zone. This agrees with the larger population of vortices found in this time span with respect to that computed in the fully turbulent regime. Additionally, we show that the presence of coherent *hairpin* vortices upstream the peak zone (i.e. before the peak) play a key role in the peak of the friction coefficient because they generate streamwise vortices (small scales). Downstream of the peak zone (i.e. after the peak), these vortices lose their coherence and the generation of small scales decays to the level found in the fully developed turbulent regime.

## 1 INTRODUCTION

The physical phenomenon of the laminar-turbulent transition in a fluid flow is a non-completely understood topic in the scientific community even for flows in simple geometries such as pipes or rectangular channels (Sano and Tamai, 2016; Lorenzini and Salvigni, 2010; Benhamou and Galanis, 2004). It is also of interest in the engineering field because parameters like the friction coefficient and the heat transfer coefficient have a strong variation along the transition (Minkowycz et al., 2009; Abraham et al., 2010, 2011).

The most common mechanism employed to yield the transition is the one that uses a finite small disturbance known as Tollmien-Schlichting waves or TS waves (Tolmmien, 1929; Schlichting, 1933). It was verified experimentally for the first time in a boundary layer flow by Schubauer and Skramstad (1947) and in channel flow by Nishioka et al. (1975). In this process, the transition starts with a linear growth of the TS wave perturbation, known in the literature as the primary instability and well described by the classical linear theory (Drazin, 1981, 2002; Schmid and Henningson, 2001). Then, the process continues with the perturbation of the primary instability by means of oblique waves, known in the literature as the secondary instability (i.e., the finite-amplitude TS waves are susceptible to three-dimensional infinitesimal oblique waves). This process can be described using the Floquet Theory (Orszag and Patera, 1983; Herbert, 1983b,a, 1988), which can predict the generation of the aligned (ordered) $\Lambda$-vortex pattern (known in the literature as the $K$-type transition (Klebanoff et al., 1962)) or the staggered $\Lambda$-vortex pattern (known in the literature as the $H$-type transition (Herbert, 1988)). This mechanism is well described in the literature as for example in Liu and Liu (1995); Chen and Liu (2011); Lu and Liu (2012); Machaca Abregu et al. (2022).

The late stage of the transitional process is characterized by the formation of $\Lambda$-vortices induced by the secondary instability. In this stage, the formation of a detached shear layer between the legs of the $\Lambda$-vortex is present and generates a *ring*-type vortex at its tip. The *ring*-type vortex with the legs of the $\Lambda$-vortex is known in the literature, after Theodorsen (Theodorsen, 1952), as a *hairpin* vortex and is composed by three parts: head, neck and two legs (Adrian et al., 2000; Wang et al., 2016; Machaca Abregu and Teruel, 2016). The *hairpin*-vortex gives place to the super-late stage or the *spike*-stage (Schlatter et al., 2004), where high-velocity fluctuations are present near the walls. These vortices yield downward jets (sweep), which move high energy from the bulk of the flow towards the wall, and upward jets (ejection), which carry low-velocity flow patches from the wall towards the bulk (Borodulin et al., 2002; Guo et al., 2010). The principal characteristic of the *ring* vortex is that near the neck of the *hairpin* vortex the sweep-ejection mechanism yields high shear layer areas that are unstable and yield small scales structures (Lu et al., 2012) (i.e. small scales structures are generated by multilevel positive *spikes* instead of large vortex breakdown (Lu and Liu, 2012)). Then the sweep-ejection mechanism mixes the flow yielding large shear layer areas that result in an increase of the friction coefficient. This process continues until the vortices lose their coherence (Lu and Liu, 2012) to give place to the fully turbulent state.

For the case of internal flows (channel or pipe flow), in the last stage of the transitional process it is commonly found the presence of a peak in the evolution of the friction coefficient (Gilbert and Kleiser, 1985; Zang and Krist, 1989; Piomelli and Zang, 1991; Sandham and Kleiser, 1992; Luo and Hui, 2004; Schlatter et al., 2006; He and Seddighi, 2013; Cherubini et al., 2021). The physics behind this characteristic is not well understood. One investigation that gives insight into this aspect was carried out by Wu et al. (2020) to show that the peak zone in the pipe transitional flow is associated with viscous motion because the mid-to-high

frequency content of the energy spectra exceeds the corresponding levels in fully developed turbulence (Wu et al., 2020).

In the present contribution DNS is carried out to simulate the temporal K-type channel flow transition. The analysis of this data allows us to obtain insight regarding the physics involved in the peak of the evolution of the friction coefficient. In section 2 the numerical method and the governing equations are presented. Next, the balance of the friction coefficient is calculated using the *Fukagata, Iwamoto and Kasagi* (FIK) identity. Later, the physical phenomenon of the friction coefficient is discussed using the current knowledge of the *hairpin* vortex growth and the budget of the turbulent kinetic energy. Finally, conclusions are drawn in the last section.

## 2 NUMERICAL METHOD

The finite difference code Incompact3d (Laizet and Lamballais, 2009; Laizet et al., 2010) is used to solve the incompressible and dimensionless Navier-Stokes equations, written in Cartesian coordinates as:

$$\frac{\partial \vec{u}}{\partial t} + \frac{1}{2}(\nabla(\vec{u} \otimes \vec{u}) + (\vec{u} \cdot \nabla)\vec{u}) = -\nabla p + \frac{1}{Re}\nabla^2 \vec{u}, \tag{1}$$

$$\nabla \cdot \vec{u} = 0, \tag{2}$$

where the distance $\vec{x}$, instantaneous velocity $\vec{u}$, pressure $p$ and time $t$ are dimensioned with the channel half-height $h$, the maximum velocity in the streamwise direction $U_o$, the constant density $\rho$ and the constant kinematic viscosity $\nu$. Therefore, $Re$ is the Reynolds number based on $U_o$ and $h$. For the spatial differentiation sixth-order centered compact schemes are used, and the time integration is performed using a third-order Adams-Bashforth scheme. For more information about the code Incompact3d visit http://www.incompact3d.com/.

The flow is simulated in a channel flow geometry and for a constant flow rate (CFR). The simulated domain is a parallel channel flow (see Fig. ( 1)) with the $x$-coordinate chosen as the streamwise direction. No-slip boundary conditions are ensured in a conventional way at the top and bottom of the computational domain ($y = 0, 2$) imposing a Dirichlet condition on the velocity. In the spanwise direction ($z$), periodicity is assumed.

In this work, the parallel-flow assumption is taken into consideration assuming periodicity in the streamwise direction to study the temporal growth of a perturbation. The perturbation imposed at the initial condition (Zang and Krist, 1989) is calculated with the eigenfunctions of the most dangerous solution of the Orr-Sommerfeld and Squire eigenvalue problem. Then the initial condition in Xcompact3d code is prescribed as:

$$\vec{U} + \vec{\tilde{u}}, \tag{3}$$

where $\vec{U} = (U(y), 0, 0)$ is the Poiseuille laminar flow (i.e. base flow) and $\vec{\tilde{u}} = (\tilde{u}, \tilde{v}, \tilde{w})$ is the perturbation given by:

$$\begin{aligned} \vec{\tilde{u}}(x, y, z, t = 0) &= A_{2d}\mathbb{R}[(\vec{\hat{u}}_{2d}(y))e^{i\alpha_{r2d}t}] \\ +\frac{1}{2}A_{3d}\mathbb{R}[(\vec{\hat{u}}^{+}_{r3d}(y))e^{i(\alpha_{r3d}x+\beta z)}] &+ \frac{1}{2}A_{3d}\mathbb{R}[(\vec{\hat{u}}^{-}_{r3d}(y))e^{i(\alpha_{r3d}x+\beta z)}], \end{aligned} \tag{4}$$

where $A_{2d}$ and $A_{3d}$ are the amplitude of the bi-dimensional (TS waves) and oblique waves respectively. The complex eigenfunctions, $\vec{\hat{u}}_{2d}$ and $\vec{\hat{u}}_{3d}$, are calculated solving the associated

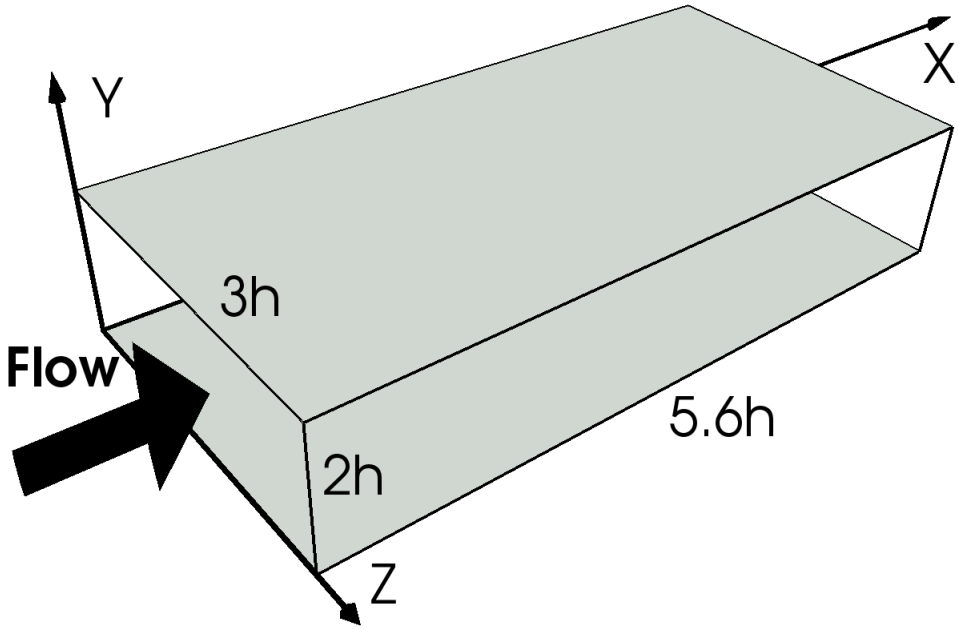


Figure 1: Computational domain.

Orr-Sommerfeld and Squire eigenvalue problem for a given $Re$, wave number in the $z$-direction ($\beta$), and the wave number in $x$-direction in two and three dimensions, $\alpha_{2d}$ and $\alpha_{3d}$, respectively. In this study the eigenfunctions have been normalized so that the maximum amplitude of their streamwise component is one for a zero phase-shift. The upper indexes + and − correspond to the eigenfunctions calculated for $\beta > 0$ and $\beta < 0$, respectively. It is well known that perturbations with $\alpha_{r3d} = \alpha_{r2d}$ yield K-type instabilities. This transition type is used in the present calculation with perturbation parameters given by $A_{2d} = 0.06$, $A_{3d} = 0.001$, $\alpha_{2d} = \alpha_{3d} = 1.12$, $\beta = \pm 2.0944$ and $Re = 5000$, that have been widely used in the literature (Schlatter et al., 2004; Schlatter, 2005; Gilbert and Kleiser, 1985; Sandham and Kleiser, 1992).

DNS is performed in a computational domain $L_x \times L_y \times L_z = \frac{2\pi}{\alpha} \times 2 \times \frac{2\pi}{\beta} = 5.6 \times 2 \times 2.99$ with a discretization of $n_x \times n_y \times n_z = 160 \times 161 \times 160$ points in the streamwise, wall-normal and spanwise directions, respectively. The discretization of the domain is homogeneous in $x$ and $z$, the periodic directions, and slightly stretched on the wall-normal direction. For fully developed turbulent regime, the $Re_\tau \approx 210$ and the near-wall resolution of the grid is given in plus unit by $x^+ = 7.4$, $y^+ = 0.9$ and $z^+ = 3.9$. Computation was carried out in the cluster of the Department of Computational Mechanics of the Bariloche Atomic Center employing one node (20 cores $XeonE52660V3@2.6GHz$). The typical run lasted approximately 100 clock-wall hours.

### 2.1 Validation

In Fig. (2a) the time evolution of $Re_\tau$ (a quantity proportional to square root of the friction coefficient (Quadrio et al., 2016)) is shown. Present results are in good agreement with reference data also included in the figure (Zang et al., 1990; Schlatter, 2005). It can be seen that this quantity has approximately a constant value until $t \approx 100$. Before this time the primary instability, the second instability and the late-stage of the transition take place (Sandham and Kleiser, 1992; Zang and Krist, 1989). Then, the friction coefficient increases its value to reach a peak at $t \approx 172$. This region is known as the super-late stage or *spike* stage due to the presence

of high-velocity fluctuations (Schlatter et al., 2004; Machaca Abregu et al., 2022) generated by *hairpin*-vortices. Finally, $Re_\tau$ decays to its fully developed turbulent value that is reached at $t \approx 210$. This region is known in the literature as the post-transitional zone.

Another quantity of interest in the evolution of the flow regime is the shape factor $H$ which is shown in Fig. (2b) (this parameter gives an idea of the flatness of the streamwise velocity profile). This quantity is also compared with Zang et al. (1990) and Schlatter (2005) to show good agreement with the present calculation.

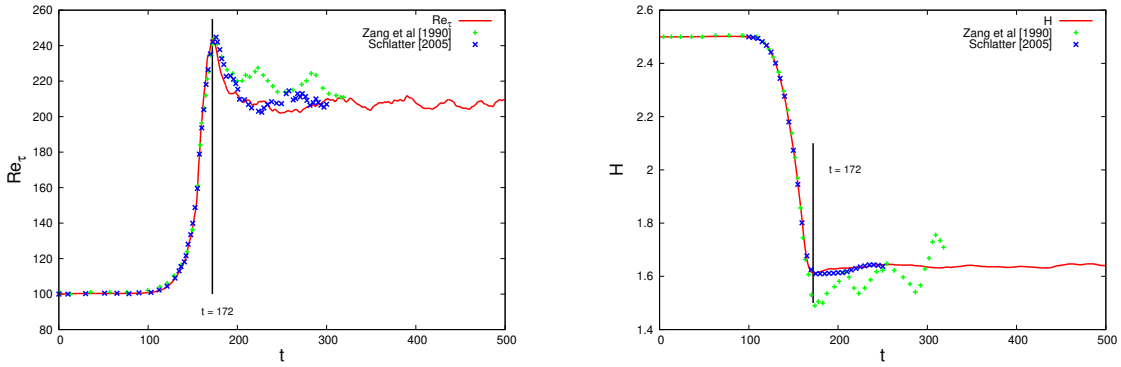


(a) Friction Reynolds number $Re_\tau$. (b) Shape factor $H$.

Figure 2: Time evolution of the friction Reynolds number $Re_\tau$ (a) and shape factor $H$ (b) for K-type transition at $Re = 5000$. —Present results, + Zang et al. (1990), and × Schlatter (2005).

## 3 RESULTS

### 3.1 Friction coefficient decomposition

The friction coefficient $C_f$ in a plane channel flow is defined in dimensional units as :

$$C_f = \frac{\mu \frac{\partial \langle u^* \rangle}{\partial y^*}\Big|_{y^*=0}}{\frac{1}{2}\rho U_0^2}, \tag{5}$$

where $(*)$ refers to dimensional units, and $\langle\rangle$ means averaged in streamwise ($x$) and spanwise ($z$) directions. This equation can be rewritten in non-dimensional units as:

$$C_f = \frac{2}{Re}\frac{\partial \langle u \rangle}{\partial y}\Big|_{y=0}. \tag{6}$$

To analyze the physics of the peak in the friction coefficient it is useful to analyze the contribution of the turbulent shear stress, which is closely related to the near-wall vortical structures (Kasagi et al., 1995). These vortical structures generate the sweep-ejection mechanism that yields high-shear layer areas near the wall. This can be carried out employing the FIK identity (Fukagata et al., 2002; Kasagi and Fukagata, 2006; Renard and Deck, 2016; Chen et al., 2021), which can be derived from the streamwise component of the Reynolds averaged Navier-Stokes equation:

$$\frac{\partial \langle u \rangle}{\partial t} = -\frac{\partial \langle p \rangle}{\partial x} + \frac{1}{Re}\frac{\partial^2 \langle u \rangle}{\partial y^2} - \frac{\partial \langle v'u' \rangle}{\partial y}. \tag{7}$$

Integrating Eq. (7) over $y$ one can obtain:

$$\int_0^1 \frac{\partial \langle p \rangle}{\partial x} \partial y = -\frac{C_f}{2}. \tag{8}$$

And using Eq. (8) into Eq. (7) and then applying the tripple integration $\int_0^1 \int_0^y \int_0^y$, the FIK identity can be obtained for the temporal transitional channel flow:

$$C_f = 6\frac{u_b}{Re} - 6\int_0^1 (1-y)\langle v'u' \rangle dy - 3\int_0^1 (1-y)^2 \frac{\partial \langle u \rangle}{\partial t} dy, \tag{9}$$

where $u_b = \int_0^1 \langle u \rangle dy$ is the bulk velocity. The first term of the right-hand side of Eq. (9) is recognized as the contribution of the laminar regime to the friction coefficient, the second one as the contribution of the Reynolds shear stress and finally, the third one, as the temporal contribution.

In Fig. (3a) the time evolution of the friction coefficient ($C_f$) and its different contributions are shown. For the sake of verification, it is also plotted the sum of the three components of the right-hand side of Eq. (9) ($All$).

The $C_f$ has approximately a constant value until $t \approx 100$, in this region the principal component of the friction coefficient is the laminar component. Then it increases its value to reach a peak at $t \approx 172$ due to the contribution of the shear stress and temporal terms. In the turbulent region ($t > 210$), the friction coefficient is approximately $0.0035$, which is in good agreement with the value reported in the literature (Schlatter et al., 2004; Zang et al., 1990).

The physics behind the peak of the friction coefficient can be analyzed with the analysis of the Reynolds shear stress. At $t \approx 100$, the Reynolds shear stress starts to increase its value showing that the turbulence intensity increases rapidly. Then it peaks, upstream of the friction coefficient peak and has an intensity greater than that corresponding to the fully developed turbulent value in the time span of $150 \lesssim t \lesssim 210$ indicating the presence of a large population of streamwise vortices. The temporal term plays a key role, also in the physics of the peak, but it does not play a significant role after the peak of the friction coefficient.

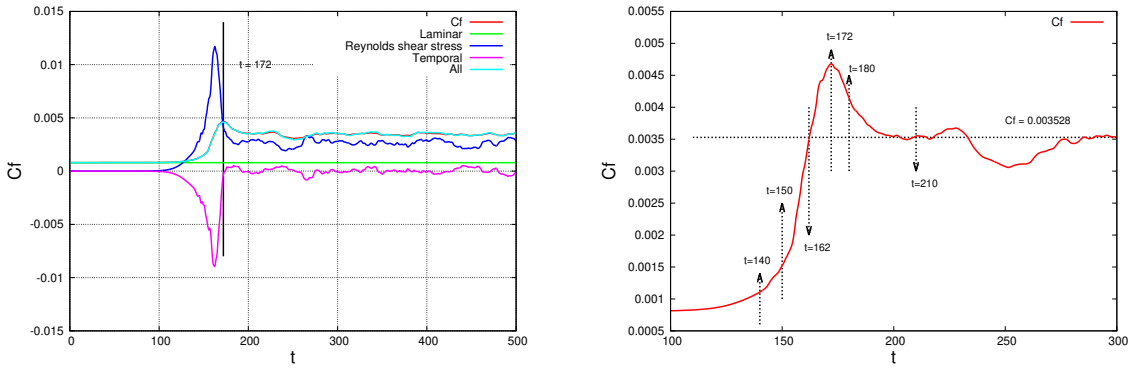


(a) Components of the friction coefficient.

(b) Friction coefficient.

Figure 3: a) Temporal evolution of the friction coefficient and its components according to the FIK identity. —$C_f$, —Laminar, —Reynols shear stress, —Temporal, —sum of the $C_f$ terms (All). b) Zoom of the $C_f$, where the fully developed value in the turbulent regime ($C_f = 0.0035$) and some particular times downstream $t \approx 100$ are indicated.

### 3.2 Vortex structures

The behavior of the friction coefficient in the temporal laminar-turbulent transition channel flow can be analyzed using the evolution of the vortex structures over time. For the sake of brevity, the structures in the quasi-linear stage (streamwise perturbation or TS waves) and in the late-stage ($\Lambda$ vortices), $t < 100$, are not shown here (the interested reader can review the following references (Sandham and Kleiser, 1992; Saiki et al., 1993; Schlatter et al., 2006)). In Fig. (4) the vortex structures are shown at the times marked in Fig. (3b). These vortices are visualized using the $\lambda_2$ vortex visualization technique (Chakraborty et al., 2005; Sengupta et al., 2019). Fig. (4a) show the *hairpin* vortices at both walls at $t = 140$ and for $\lambda_2 = -1$. These vortices are symmetric around the $z = 1.5$ plane and their legs are near the walls but the heads (*ring* vortices) are far away from them (note the $y = 0.5$ plane colored in the Fig. (4)). At this time the vortices are still located near the $z = 1.5$ plane and their intensity in magnitude is lower than that found at later times. Additionally, the increase of the friction coefficient is moderate respect to its laminar value. In Fig. (4b) (at time $t = 150$ and for $\lambda_2 = -4$), the vortices are still near $z = 1.5$, but the interaction between both walls is evident. Also, the population of the streamwise vortices near the walls is higher than that found at $t = 140$. The friction coefficient also increases more rapidly than before. At $t = 160$ (see Fig. (4c)), the vortex packet starts to spread along $z$ direction with the generation of more streamwise vortices near the walls. Near the peak of the friction coefficient ($t = 170$), the vortex structures populate completely the channel section. At $t = 180$ (see Fig. (4e)), there are remnants of the *ring* vortices which still populate the centerline of the channel. At this instantaneous time, the friction coefficient decreases rapidly from its peak. Finally, at $t = 210$, the streamwise vortex structures are located near the wall and there are no coherent *ring* vortices in the bulk of the flow.

Using the description of the vortex structures near the peak of the friction coefficient, it is found that the coherent *hairpin* vortices at $t < 172$ play a key role in the increase of the friction coefficient because they yield streamwise vortices due to the sweep-ejection mechanism increasing the Reynolds shear stress. At $t > 172$, the coherence of the *ring* vortex structure is not sustained, then the streamwise vortices are not generated and the friction coefficient decays.

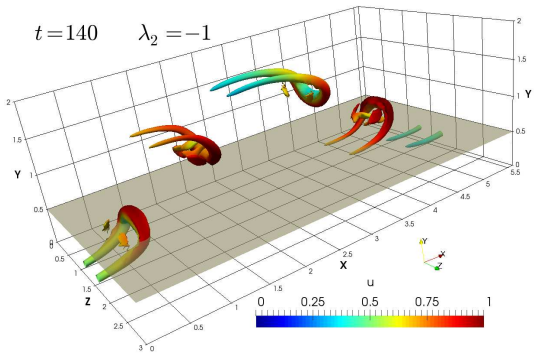


(a) $t$ = 140.

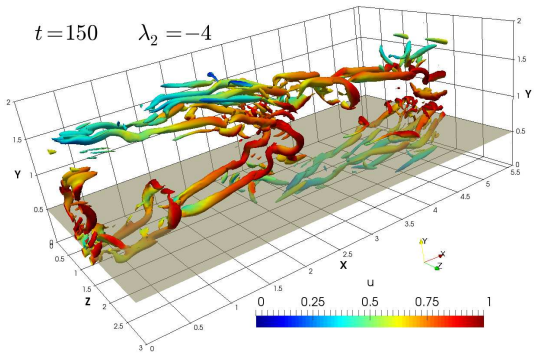


(b) $t$ = 150.

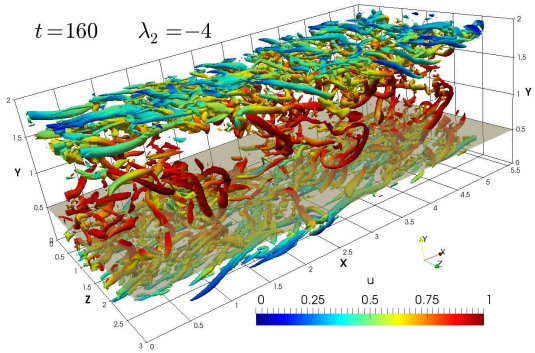


(c) $t$ = 160.

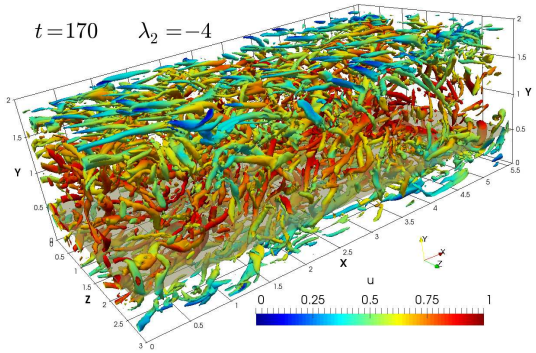


(d) $t$ = 170.

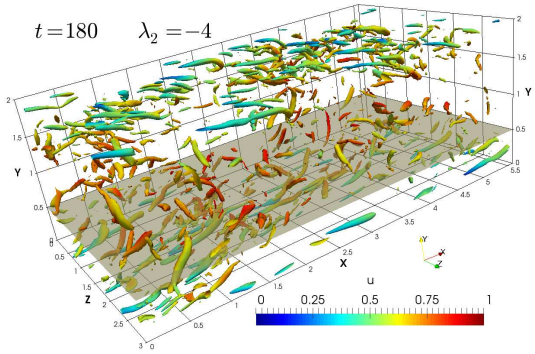


(e) $t$ = 180.

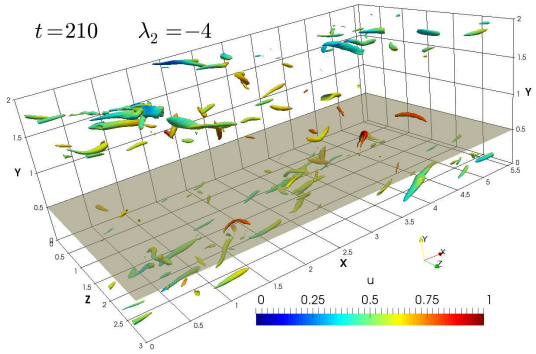


(f) $t$ = 210.

Figure 4: Vortex structures at different instantaneous times for $t > 100$.

### 3.3 Budget of the $TKE$

An important quantity to analyze the contribution of the vortical structures to the friction coefficient is the turbulent dissipation (Vassilicos, 2015). For this reason, the budget of the turbulent kinetic energy ($TKE = \frac{\langle u'u'\rangle+\langle v'v'\rangle+\langle w'w'\rangle}{2}$) in the transitional region is analyzed. The

budget of the $TKE$ is shown in the following equation:

$$\begin{aligned}
\frac{\partial TKE}{\partial t} + \langle u_j \rangle \frac{\partial TKE}{\partial x_j} = & -\langle u_j' u_i' \rangle \frac{\partial \langle u_i \rangle}{\partial x_j} \quad ...(P) \\
& -\frac{1}{2} \frac{\partial \langle u_i' u_i' u_j' \rangle}{\partial x_j} \quad ...(TD) \\
& -\langle u_i' \frac{\partial p'}{\partial x_i} \rangle \quad ...(V - PGCorr.) \\
& +\frac{1}{Re} \frac{\partial^2 TKE}{\partial x_j \partial x_j} \quad ...(VD) \\
& -\frac{1}{Re} \langle \frac{\partial u_i'}{\partial x_j} \frac{\partial u_i'}{\partial x_j} \rangle \quad ...(Diss.)
\end{aligned} \tag{10}$$

where the components of the left-hand side of the Eq. (10) are the temporal and the convection terms, respectively. The convection term, in the present case, is only $\langle v \rangle \frac{\partial TKE}{\partial y}$ because the flow is homogeneous in $x$ and $z$ directions. As the wall-normal velocity, $\langle v \rangle$, is zero, the convection term is not relevant. The terms of the right-hand side of the Eq. (10) are respectively: Production ($P$), Turbulent Diffusion ($TD$), Velocity-Pressure Gradient correlation ($V - PGCorr.$), Viscous Diffusion ($VD$) and Dissipation ($Diss.$).

In Fig. (5) the six components of the TKE budget are shown in nondimensional units (averaged in streamwise, spanwise and wall-normal directions). It can be seen that for $t < 100$, in the scale of the figure all terms are approximately null, which is reflected in the constant value of the friction coefficient. From $t \approx 100$ to $t \approx 210$, the dominant terms are the production, dissipation and temporal terms, and the other terms are of lower order. First, it is noted that the production term is greater than the dissipation term, which is a consequence of the transfer of the energy from the mean flow to small scales due to the presence of the coherent *ring* vortices (see Fig. (4)). When these vortices lose their coherence, the production of small scales decreases (Lu and Liu, 2012). This mechanism is reflected in the production and dissipation terms, where for $t > 172$, the dissipation term is greater, in magnitude, than the production term, showing that energy is being dissipated due to the presence of small scales near the centerline (remanents of *ring* vortices) and near walls as can be seen in Fig. (4e) at $t = 180$ (Vassilicos, 2015). For $t > 210$, the remnants of *ring* vortices near the channel center are dissipated to give place to the fully developed turbulent state. In this region both, production and dissipation terms, are balanced, and the other components of the budget are approximately zero.

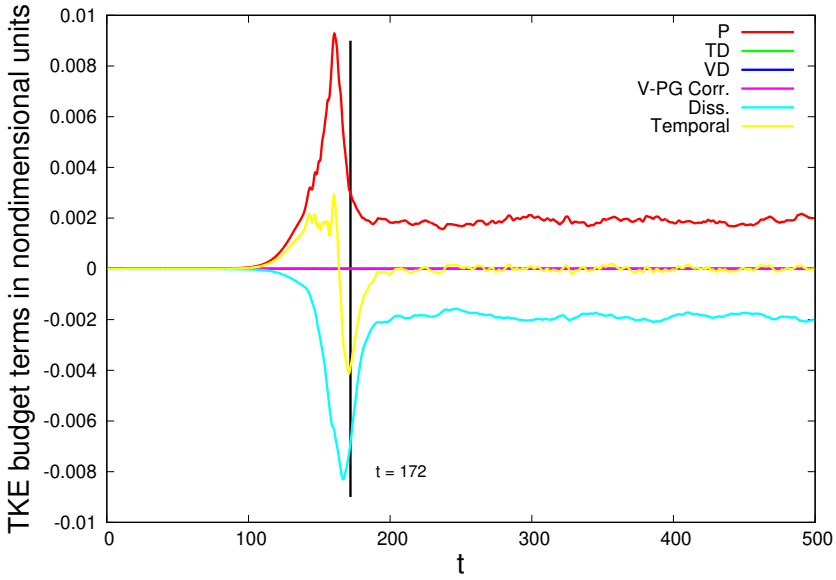


Figure 5: TKE budget terms in non-dimensional units averaged in streamwise, spanwise and wall-normal directions. —Production, —Turbulent diffusion, —Viscous diffusion, —Velocity-pressure gradient correlation, —Dissipation and —Temporal.

## 4 SUMMARY AND CONCLUSIONS

Direct numerical simulation of the temporal laminar-turbulent K-type transition was carried out to study the peak of the friction coefficient that is present in the super-late stage of the transitional region. The configuration of the flow was a channel flow with periodic boundary conditions in streamwise and spanwise directions. The simulation was carried out solving the Navier-Stokes equations for incompressible flow using the Xcompact3d code. For the temporal simulation, the initial condition was a Poiseuille laminar flow with a perturbation calculated solving the Orr-Sommrfeld and Squire equation for the following parameters: $A_{2d} = 3\%, A_{3d} = 0.1\%, \alpha_{2d} = \alpha_{3d} = 1.12, \beta = \pm 2.1$ and $Re = 5000$. To validate the present results, the time evolution of the friction Reynolds number and the shape factor was calculated and compared with good agreement with the results of Zang et al. (1990) and Schlatter (2005).

The analysis of the evolution of the friction coefficient $C_f$ was made using the FIK identity. It was found that the Reynolds shear stress term plays a key role in the evolution of this quantity in the transition region and in the turbulent one. This quantity has a greater value near the peak of the friction coefficient than that corresponding to the fully developed turbulent regime. This high value is explained considering the large population of vortices at $t = 160, 170$ and $t = 180$. These coherent *hairpin* vortices generate streamwise vortices and an overproduction of TKE.

The behavior of the peak zone was also analyzed considering the analysis of the budget of the TKE. The time evolution of the six terms of the budget was calculated, where the most important terms were the production, dissipation and temporal terms. For $t \approx 100$ to $t \approx 170$, the magnitude of the production term indicates an overproduction of TKE due to the presence of coherent *hairpin* vortices. When these vortices lose their coherence, the production of small scales decreases, which is reflected in the production and dissipation term near the peak of the friction coefficient. For $t > 172$ the dissipation term was greater in magnitude than the production term, indicating that the energy is dissipated due to the presence of small scales in the channel domain but the generation of small scales due to the presence of the *ring* vortices near

the centerline has diminished. For $t > 210$, the production and dissipation terms are balanced and we only found streamwise vortices near the channel walls, which is a characteristic of the fully turbulent regime.

## REFERENCES


Abraham J.P., Sparrow E., and Minkowycz W.J. Internal-flow Nusselt numbers for the low-Reynolds-number end of the laminar-to-turbulent transition regime. *International Journal of Heat and Mass Transfer*, 54:584–588, 2011.

Abraham J.P., Sparrow E.M., Tong J., and Bettenhausen D. Internal flows which transist from turbulent through intermittent to laminar. *International Journal of Thermal Sciences*, 49:256–263, 2010.

Adrian R.J., Meinhart C.D., and Tomkins C.D. Vortex organization in the outer region of a turbulent boundary layer. *Phys. Fluids*, 422:1–54, 2000.

Benhamou B. L.A. and Galanis N. Transition to turbulence: The case of a pipe in radial oscillations. *International Journal of Thermal Sciences*, 43:1141–1151, 2004.

Borodulin V.I., Gaponenko V.R., and Kachanov Y.S. Late-stage transitional boundary-layer structures. Direct numerical simulations and experiment. *Theoret. Comput. Fluids Dynamics*, 15:317–337, 2002.

Chakraborty P., Balachandar S., and Adrian R.J. On the relationships between local vortex identification schemes. *J. Fluid Mech.*, 535:189–214, 2005.

Chen L. and Liu C. Numerical study on mechanisms of second sweep and positive spikes in transitional flow on a flat plate. *Computers and Fluids*, 40:28–41, 2011.

Chen X., Yao J., and Hussain F. Theoretical framework for energy flux analysis of channels under drag control. *Physical Review Fluids*, 6:013902, 2021.

Cherubini S., Picella F., and Robinet J.C. Variational nonlinear optimization in fluid dynamics: the case of channel flow with superhydrophobic walls. *Mathematics*, 9(53):1–24, 2021.

Drazin P.G. *Hydrodynamic Stability*. Cambridge University Press, 1981.

Drazin P.G. *Introduction to Hydrodynamic Stability*. Cambridge University Press, 2002.

Fukagata K., Iwamoto K., and Kasagi N. Contribution of Reynolds stress distribution to the skin friction in wall-bounded flows. *Phys. Fluids*, 14:L73, 2002.

Gilbert N. and Kleiser L. Subcritical transition to turbulence in channel flow. In *Direct and Large Eddy Simulation of Turbulence*. Hemisphere, Washington, DC, 1985.

Guo H., Borodulin V.I., Kachanov Y.S., Pan C., Wang J.J., Lian Q.X., and Wang S.F. Nature of sweep and ejection events in transitional and turbulent boundary layers. *Journal of Turbulens*, 11(34):1–51, 2010.

He S. and Seddighi M. Turbulence in transient channel flow. *J. Fluid Mech.*, 715:60–102, 2013.

Herbert T. Secondary instability of plane channel flow to subharmonic three-dimensional disturbances. *Phys. Fluids*, 26:871–874, 1983a.

Herbert T. Stability of plane Poiseuille flow-theory and experiment. *Fluid Dynamics Trans.*, 11:77–126, 1983b.

Herbert T. Secondary Instability of Boundary Layers. *Annual Review of Fluid Mechanics*, 20:487–526, 1988.

Kasagi N. and Fukagata K. The FIK identity and its implication for turbulent skin friction control. In *Transition and Turbulence Control*. World Scientific, Singapore, 2006.

Kasagi N., Sumitani Y., Suzuki Y., and Iida O. Kinematics of the quasi-coherent vortical structure in near-wall turbulence. *Int. J. Heat Fluid Flow*, 16:2–10, 1995.

Klebanoff P., Tidstrom K., and Sargent L. The three-dimensional nature of boundary-layer

instability. *Journal of Fluid Mechanics*, 12:1–34, 1962.

Laizet S. and Lamballais E. High-order compact schemes for incompressible flows: A simple and efficient method with quasi-spectral accuracy. *J.C. Physics*, 228(16):5989–6015, 2009.

Laizet S., Lamballais E., and Vassilicos J.C. A numerical estrategy to combine high-order schemes, complex geometry and parallel computing for high resollution DNS of fractal generated turbulence. *Computers and Fluids*, 39(3):471–484, 2010.

Liu C. and Liu Z. Multigrid mapping and box relaxation for simulation of the whole process of flow transition in 3D boundary layers. *Journal of Computational Physics*, 119(2):325–341, 1995.

Lorenzini M. M.G.L. and Salvigni S. Laminar, transitional and turbulent friction factors for gas flows in smooth and rough microtubes. *International Journal of Thermal Sciences.*, 49:248–255, 2010.

Lu P. and Liu C. DNS study on mechanism of small length scale generation in late boundary layer transition. *Physica D*, 241:11–24, 2012.

Lu P., Thapa M., and Liu C. Surface friction and boundary layer thickening in transitional flow. *Advances in Modeling of Fluid Dynamics*, pages 1–14, 2012.

Luo J. and Hui L. Influence of small imperfections on the stability of plane poiseuille flow: A theoretical model and direct numerical simulation. *Physics of Fluids*, 16:8, 2004.

Machaca Abregu W.I. and Teruel F.E. *Estudio de las estructuras de vorticidad en la transición espacial laminar-turbulenta en canales angostos*. ENIEF 2016, Córdoba, Argentina, 2016.

Machaca Abregu W.I., Teruel F.E., and Dari E. Study of the spatial transition in a plane channel flow. *Computer and Fluids*, 247:105650, 2022. doi:https://doi.org/10.1016/j.compfluid.2022.105650.

Minkowycz W.J., Abraham J.P., and Sparrow E.M. Numerical simulation of laminar breakdown and subsequent intermittent and turbulent flow in parallel-plate channels: Effects of inlet velocity profile and turbulence intensity. *International Journal of Heat and Mass Transfer*, 52:4040–4046, 2009.

Nishioka M., Iida S., and Ichikawa Y. An experimental investigation of the stability of plane Poiseuille flow. *J. Fluid Mech.*, 72(4):731–751, 1975.

Orszag S.A. and Patera A.T. Secondary instability of wall-bounded shear flows. *J. Fluid Mech.*, 128:347–385, 1983.

Piomelli U. and Zang T.A. Large-eddy simulation of transitional channel flow. *Computer Physics Communications*, 65:224–230, 1991.

Quadrio M., Frohnapfel B., and Hasegawa Y. Does the choice of the forcing term affect flow statistics in DNS of turbulent channel flow. *European Journal of Mechanics B/Fluids*, 55:286–293, 2016.

Renard N. and Deck S. A theoretical decomposition of mean skin friction generation into physical phenomena across the boundary layer. *J. Fluid Mech.*, 790:339, 2016.

Saiki E., Biringen S., Danabasoglu G., and Streett C. Spatial simulation of secondary instability in plane channel flow: comparison of k- and h-type disturbances. *Journal of Fluid Mechanics*, 253:485–507, 1993.

Sandham N.D. and Kleiser L. The late stages of transition to turbulence in channel flow. *J. Fluid Mech.*, 245:319–348, 1992.

Sano M. and Tamai K. A universal transition to turbulence in channel flow. *Nature Physics*, 12:249–254, 2016.

Schlatter P. *Large-Eddy simulation of transition and turbulence in wall-bounded shear flow.* PhD tesis, Swiss Federal Institute of Technology, Zurich, 2005.

Schlatter P., Stolz S., and Kleiser L. Les of transitional flows using the approximate deconvolution model. *International Journal of Heat and Fluid Flow*, 25:549–558, 2004.

Schlatter P., Stolz S., and Kleiser L. Large-eddy simulation of spatial transition in plane channel flow. *Journal of Turbulence*, 7:33, 2006.

Schlichting H. Zur Entstehung der Turbulenz bei der Plattenstromung. *Z. Angew. Math. Mech.*, 13:171–174, 1933.

Schmid P.J. and Henningson D.S. Stability and Transition in Shear Flows. In *Applied Mathematical Sciences*, volume 142. Springer, 2001.

Schubauer G.B. and Skramstad H.K. Laminar boundary layer oscillations and the stability of laminar flow. *J. Aeronaut. Sci.*, 14:69–78, 1947.

Sengupta T.K., Sharma P.K., Sengupta A., and Suman V.K. Tracking disturbances in transitional and turbulent flows: Coherent structures. *Physics of Fluids*, 31:124106, 2019.

Theodorsen T. Mechanism of turbulence. In *Proc. Second Midwestern Conj. of Fluid Mechanics*, pages 1–19. Ohio State University, Columbus, Ohio, 1952.

Tolmmien W. Uber die Entstehung der Turbulenz. *Nachr. Ges. Will. Gottingen*, 1:21–44, 1929.

Vassilicos J.C. Dissipation in turbulent flows. *Annu. Rev. Fluid Mech.*, 47:95, 2015.

Wang Y., Al-Dujaly H., Yan Y., and Zhao N. Physics of multiple level hairpin vortex structures in turbulence. *Physics, Mechanics and Astronomy, Science China*, 59(2):1–11, 2016.

Wu X., Moin P., and Adrian R.J. Laminar to fully turbulent flow in a pipe: scalar patches, structural duality of turbulent spots and transitional overshoot. *J. Fluid Mech.*, 896 (A9):1–27, 2020.

Zang T.A., Gilbert N., and Kleiser L. Direct numerical simulation of the transitional zone. In *Instability and Transition*, volume 2. Springer, New York, 1990.

Zang T.A. and Krist S.E. Numerical experiments on stability and transition in plane channel flow. *Theoret. Comput. Fluid Dynamics*, 1:41–64, 1989.